Journal of Biomedical Optics

SPIEDigitalLibrary.org/jbo

Noise characteristics of heterodyne/homodyne frequency-domain measurements

Dongyel Kang
Matthew A. Kupinski

SPIE

Noise characteristics of heterodyne/homodyne frequency-domain measurements

Dongyel Kang and Matthew A. Kupinski
University of Arizona, College of Optical Sciences, 1630 E. University Boulevard, Tucson, Arizona 85721

Abstract. We theoretically develop and experimentally validate the noise characteristics of heterodyne and/or homodyne measurements that are widely used in frequency-domain diffusive imaging. The mean and covariance of the modulated heterodyne output are derived by adapting the random amplification of a temporal point process. A multinomial selection rule is applied to the result of the temporal noise analysis to additionally model the spatial distribution of intensified photons measured by a charge-coupled device (CCD), which shows that the photon detection efficiency of CCD pixels plays an important role in the noise property of detected photons. The approach of using a multinomial probability law is validated from experimental results. Also, experimentally measured characteristics of means and variances of homodyne outputs are in agreement with the developed theory. The developed noise model can be applied to all photon amplification processes. [DOI: 10.1117/1.JBO.17.1.015002]

Keywords: biomedical optics; heterodyning; homodyning; image intensifiers; medical imaging; noise.

Paper 11345 received Jul. 5, 2011; revised manuscript received Oct. 27, 2011; accepted for publication Nov. 4, 2011; published online Feb. 7, 2012.

1 Introduction

When an intensity-modulated beam is used to illuminate diffusive media, the modulation amplitude and phase of the beam are attenuated and delayed, respectively, due to absorption and scattering inside the medium. The amplitude attenuation is caused by both scattering and absorption, whereas the phase delay is mainly related to scattering. Because the typical modulation frequency range in frequency-domain diffusive imaging is from tens of megahertz up to a gigahertz,[1–3] a very high bandwidth detector is required to correctly measure modulation amplitudes and phases. In additional to measuring the frequency-response information, it has been shown that obtaining large datasets using detector arrays also improves diffusive imaging performance.[4,5] It is almost impossible to achieve the high bandwidths required in frequency-domain measurements with high-density detector arrays such as charge-coupled device (CCD) or complementary metal-oxide-semiconductor (CMOS) sensors. Heterodyne and/or homodyne (hetero/homodyne) methods extract the amplitude and phase information by converting the rapidly modulating output beam into a beat-frequency modulation mode using gain-modulated amplifiers, such as an image intensifier (IIN) and photo multiplier (PMT).[6,7] When the gain modulation frequency is slightly different from that of a light source, the amplified output modulates at the frequency difference—a beat frequency, which is a heterodyne measurement. For a homodyne measurement, where a gain is modulated at the same frequency as a modulation source, the output is stable in time, but its irradiance is varied along the heterodyne output according to relative phases between source and gain modulations. Although time-domain measurements can also extract the frequency response of diffusive media, hetero/homodyne measurements are more widely used in diffusive imaging because of their relatively low cost and simplicity.[1,6]

In general, measuring intensity-modulated outputs improves the reconstruction algorithms and other algorithms designed to estimate tissue properties, when compared to measuring just diffused intensities (i.e., steady-state measurements).[1] For example, diffuse optical tomography (DOT), which is considered a noninvasive and cost-effective medical imaging tool, can tomographically reconstruct images of scattering and absorption coefficients up to tens of millimeters in depth.[2,3] DOT systems based on just a diffused intensity are simple and inexpensive but have significant disadvantages including the measurement variability caused by skin structure, hair, and surface roughness.[1] Furthermore, the measured diffused intensity generally cannot reconstruct a unique solution, and the crosstalk between absorption and scattering coefficients cannot be effectively separated in reconstruction processes.[8,9] A frequency-domain DOT can remedy these problems and thus improves detectability and reconstruction performance. Frequency-domain measurements are also required in fluorescent lifetime imaging (FLI), where the fluorophore lifetime is used as an important indicator of tissue characteristics.[10] Since the typical fluorescent lifetimes are a few nanoseconds and cannot be measured directly, measuring attenuated amplitude and delayed phase of modulated fluorescent photons can be used effectively to estimate the lifetime.[7,11–13] Measuring the frequency-domain information in large tissue areas using a CCD and a gain-modulated IIN can be used to generate a spatial fluorescent lifetime map of the tissue.[14]

Noise is inherent in all measurements. Even though averaging multiple measurements or increasing detector exposure time can reduce the amount of noise, these approaches are prohibited or limited in some dynamic-imaging applications and clinical situations.[1] In medical imaging, data are acquired

Address all correspondence to: Dongyel Kang, University of Arizona, College of Optical Sciences, 1630 E. University Boulevard, Tucson, Arizona 85721. Tel: +5203900979; E-mail: dkang@optics.arizona.edu

0091-3286/2012/$25.00 © 2012 SPIE

for specific purposes or tasks that include classification, such as detection of abnormalities like a tumor, and estimation of biological quantities, such as a fluorescent lifetime. Noise-contaminated data is a limiting factor in an observer's ability to perform these classification and/or estimation tasks. The noise is especially significant in diffusive medical imaging, such as DOT and FLI, because of low photon counts.[12–17] The performance of noise-contaminated systems can be evaluated quantitatively by considering figures of merit (FOMs) that are chosen to reflect an observer's ability to perform these medial-relevant tasks.[15,18] Task-based assessment of image quality evaluates and/or optimizes diffusive imaging systems by employing FOMs that assess observer performance.[18–20] Many task-based FOMs rely on the first and second moments of output data,[18,21,22] so understanding the noise property of output data is important and necessary.

Because of the importance of noise analysis in diffusive imaging, the noise characteristics of a modulation amplitude and phase for frequency-domain diffusive imaging have been previously investigated. Toronov et al.[23] mathematically derived variances of these quantities in frequency-domain DOT assuming a quantum shot noise model on the hetero/homodyne outputs. Conventional signal-to-noise ratios (SNRs) and a task-based FOM known as a Hotelling observer SNR were derived based on Toronov's result, and an optimal modulation frequency was explored in DOT systems of a single point source and CCD-based phased array.[16,23–25] In FLI, a FOM called F-value is commonly used to evaluate system performance, where the F-value is defined by first- and second-order statistics of a fluorescent lifetime.[12,13] Many investigators have optimized FLI systems by maximizing the F-value or minimally required fluorescent photon numbers for a meaningful F-number.[12,13,26] It is reasonable that the F-value is strongly dependent on the noise characteristics of modulation amplitude and/or phase in frequency-domain FLI because the fluorescent lifetime is estimated from these quantities. For all previous studies including Toronov's result, however, Gaussian or shot noise is simply considered for the statistics of modulation amplitude and phase or only shot noise is assumed for the hetero/homodyne outputs,[9,23] which might not be valid in reality. For example, the irradiance of hetero/homodyne outputs is usually high due to the photon amplification process, which is enough to ignore the effect of shot noise in a detector. Furthermore, the beat-frequency modulated output might be temporally correlated, which is seriously harmful to the assumption of quantum shot noise.

The noise properties of amplified photons for the non-modulation case have already been investigated, where incident photons are assumed to be Poisson distributed. The photon amplification in IINs and intensified CCDs (ICCDs) should be considered a random process even for a constant gain, which generally induces non-Poisson outputs for Poisson inputs.[18] Bell theoretically analyzed a noise figure for IINs with a constant gain,[27] where the noise figure was defined as the ratio of SNRs of input and output photons. He considered photons incident on a micro channel plate (MCP) in IINs or ICCDs as governed by Poisson statistics, and each photoelectron collision on the wall of the MCP generates the photoelectron distribution called Furry distribution. Moran et al.[28] theoretically derived a noise factor (NF) of ICCDs, which is defined as the square of the noise figure. He showed that variations of a NF and an output SNR are not linearly related to MCP gain, which is partially observed in experiments elsewhere.[17,29] Moran adapted a Polya distribution as a single photoelectron pulse in a MCP. Instead of photoelectron distributions in a MCP, Apanasovich and Novikov[30] analyzed the amplification process considering electron multiplication events in a MCP as random point processes and compared the theoretical model with experiments. Frenkel et al.[31] investigated variance and noise-equivalent irradiance of outputs in an ICCD using the approach of spatial point processes. Although these previous noise analyses for randomly amplified photons are mathematically sound, to the author's knowledge, noise analysis has not been performed for heterodyne/homodyne measurements where both incident beam and amplification gain are modulating. Spring and Clegg[32] briefly touch on the SNR of homodyne outputs, but gain modulation is simply substituted for the constant gain in the conventional SNR expression for PMTs.

In this paper, we theoretically derive mean and covariance properties of hetero/homodyne outputs, which are expressed with systematic parameters of hetero/homodyne measurements, such as dc and ac parts of incident primary modulation beams and modulation gain. The theoretical development includes both temporal and spatial analyses. Temporally, a hetero/homodyne measurement process is considered random amplification of a modulated temporal point process. Spatially, a multinomial selection rule is applied to model the spatial distribution of the amplified photons from MCPs to detector array pixels. Resulting from this, it is found that hetero/homodyne outputs are temporally uncorrelated and the variance oscillates like the mean in some specific conditions. We suggest experimental results of homodyne measurements that show similar characteristics with what is expected from the developed theory. Discussions for the influence of the derived noise property on frequency-domain diffusive imaging are also presented.

2 Theory for Temporal Noise Analysis

For hetero/homodyne detection processes in diffusive imaging, the diffused photons exiting an object (e.g., phantom) are captured by an imaging system, where the exit face is imaged onto a cathode of an IIN through the imaging system. The incident photons to the cathode generate photoelectrons that are injected into the MCP of the IIN, where the voltage difference between the cathode and the MCP determines the amount of injected photoelectrons. A MCP is typically composed of millions of small channels that are related to the overall resolution of an IIN. A single photoelectron collision that occurred on the wall of the MCP generates multiple photoelectrons, the number of which is proportional to the voltage applied to the MCP. The overall gain of the IIN is determined mainly by photoelectrons generated from the cathode and the MCP voltage that are independent of a cathode voltage. To achieve gain modulation in an IIN, a modulated voltage is applied to a cathode to generate modulated photoelectrons that are amplified in a MCP. The multiplied photoelectrons from the MCP are accelerated to an anode (phosphor) to generate intensified photons. The usual decay time of phosphors ranges from hundreds of nanoseconds to a few milliseconds.[33] The photons discharged from the anode are transferred to a detector array, such as a CCD or CMOS, by an appropriate imaging system. Overall, a phantom exit face and a CCD detector surface are object and image planes, respectively, of the whole frequency-domain measurement system. Resulting from this view, each CCD detector pixel is conjugate to a detection area on the exit face, the size of which is

determined by the CCD pixel size and the transverse magnification of the whole hetero/homodyne imaging system.

It is assumed that hetero/homodyne output photons are described by a temporal point process as

$$y(t) = \sum_{n=1}^{N} \sum_{k=1}^{k_n} \delta(t - t_n - \Delta t_{nk}), \tag{1}$$

where t_n is the time that n'th primary photon (diffused photon from a phantom) is absorbed on a cathode of the IIN and Δt_{nk} is the time of delay for secondary photons produced from an anode of the IIN by the n'th primary. In Eq. (1), N and k_n are numbers of primaries and secondaries, respectively; these are all random variables. The mean and covariance of the point process of Eq. (1) have been derived for the case of non-modulation input and IIN gain.[18,34] Referring to this known procedure, we will develop the mean and covariance of $y(t)$ for hetero/homodyne measurements. A mean photon arrival rate from a phantom to a cathode of the IIN is expressed as

$$a_p(t) = c_p[1 + m_p \cos(\omega_p t + \psi)], \tag{2}$$

where $\omega_p = 2\pi f_p$ and c_p, m_p, and ψ indicate dc photon rate, modulation depth that is less than 1, and modulation phase, respectively. The term f_p is a modulation frequency that is usually hundreds of megahertz in frequency-domain diffusive imaging, as mentioned in the introduction. Although c_p, m_p, and ψ are continuously varied across the phantom exit face or the cathode of the IIN, it is assumed that the amounts of variation are insignificant within the detection area conjugate to a CCD pixel, so they can be considered constant as in Eq. (2). If we assume that Poisson postulates are fulfilled for the diffused photons on the detection area, the probability density function (PDF) for the primary is[18]

$$\mathrm{pr}_{\mathrm{pri}}(t_n|a_p) = \frac{a_p(t_n)}{\bar{N}(a_p)}, \tag{3}$$

where

$$\bar{N}(a_p) = \int_0^T a_p(t)\mathrm{d}t. \tag{4}$$

Notice that the mean total number $\bar{N}(a_p)$ also modulates because of the modulating photon arrival rate, $a_p(t)$. Without losing the generality, we assume the mean photon rate in Eq. (2) is not random, which indicates that noise external to the hetero/homodyne system, such as random biological motions and respiration, will not be considered in this theoretical development.

The shift-variant temporal point spread function (PSF) of the IIN with gain modulation can be described as

$$\begin{aligned} p_d(t,t_n) &= c_g\left[1 + \sum_{g=1}^{\infty} m_g \cos(\omega_g t_n + \varphi_g)\right] \\ &\quad \times \int_{\infty} p_a^I(t,t_n')p_m^I(t_n,t_n')\mathrm{d}t_n' \\ &= c_g\left[1 + \sum_{g=1}^{\infty} m_g \cos(\omega_g t_n + \varphi_g)\right] p_d^I(t,t_n), \end{aligned} \tag{5}$$

where $p_a^I(t,t_n')$ and $p_m^I(t_n,t_n')$ are temporal PSFs of the anode and MCP of the IIN, respectively. The term $c_0[1 + \sum_{g=1}^{\infty} m_g \cos(\omega_g t_n + \varphi_g)]$ in Eq. (5) indicates a modulated photoelectron rate from the cathode for a single primary, which is equivalent to cathode gain modulation. The term ω_1 is the same as or close to ω_p in hetero/homodyne measurements. Because the modulation voltage should be applied to around the cutoff voltage of a cathode, the modulated cathode gain is generally similar to a bottom-truncated sinusoidal function rather than a perfect sinusoidal curve.[32] It is noted that for this case, the largest coefficient m_1 in the cathode modulation could be larger than 1 because c_0 is defined by averaging the modulated cathode gain. The periodic cathode gain is expanded to Fourier cosine terms,[32] as shown in Eq. (5), where the amplitude and phase of each term is indicated as $c_0 m_g$ and φ_g, respectively. From the assumption that the gain is an even and periodic function, it can be easily shown that there is no phase difference between cosine terms (we set all φ_g as zeros for simplicity) and $\omega_g = g\omega_1$, where g is an integer. The usual photocathode response time of a cathode is picoseconds to femtoseconds,[35] so the photoelectron conversion time on a cathode is ignored in Eq. (5). The time for multiplying photoelectrons in the MCP is also negligible compared with the photoelectron-photon conversion time on an anode, which is usually a few milliseconds. The random variable t for the secondary in Eq. (5) is not independent of each other because t is correlated to t_n. If t in Eq. (5) is replaced by Δt_{nk} as in Eq. (1), Δt_{nk} can be considered statistically independent and Poisson postulates are satisfied for secondaries produced from each primary.[18] With this replacement, the probability density function (PDF) for secondary photons can be written from Eq. (5) as

$$\mathrm{pr}_{\Delta t}(\Delta t_{nk}|t_n) = [\bar{k}_n(t_n)]^{-1} p_d(\Delta t_{nk} + t_n, t_n), \tag{6}$$

where the mean number of secondary photons produced by a primary is

$$\begin{aligned} \bar{k}_n(t_n) &= \int_{\infty} p_d(t,t_n)\mathrm{d}t \\ &= c_0\left[1 + \sum_{g=1}^{\infty} m_g \cos(\omega_g t_n)\right] \int_{\infty} p_d^I(t,t_n)\mathrm{d}t \\ &= c_0\left[1 + \sum_{g=1}^{\infty} m_g \cos(\omega_g t_n)\right] \bar{k}_n^I(t_n). \end{aligned} \tag{7}$$

In Eq. (7), $\bar{k}_n^I(t_n)$ indicates the mean number of amplified photons for a single photoelectron injected into the MCP. The time dependence in $\bar{k}_n^I(t_n)$ indicates a long-term MCP and/or anode variation caused by, for example, thermal instability. We are interested in the noise property of a hetero/homodyne output that is stationary in time, thus assuming $\bar{k}_n^I(t_n) \sim \bar{k}_n^I$. Also, photon and photoelectron losses, such as cathode quantum efficiency and an open area ratio of the MCP,[27] could be included in c_0 in Eq. (7).

Mean and covariance of Eq. (1) can be derived by statistically averaging the time for secondary Δt_{nk}, the number of secondaries k_n, the time for primary t_n, and the number of primaries $N(a_p)$. As a final step, averaging $a_p(t)$ would be necessary if the primary is doubly stochastic, but this is not the case as

we assumed before. As shown in the appendix, the mean and covariance are derived from Eqs. (2) to (7) as

$$\langle y(t)\rangle = c_p c_0 \int_\infty [1 + m_p \cos(\omega_p t_n + \psi)] \times \left[1 + \sum_{g=1}^{\infty} m_g \cos(\omega_g t_n + \varphi_g)\right] p_d^I(t, t_n)\mathrm{d}t_n, \quad (8)$$

and

$$K_y(t, t') = \int_\infty \{\bar{k}_n^2(t_n) + \mathrm{Var}[k_n|t_n]\} a_p(t_n)\mathrm{pr}_{\Delta t}(t, t_n) \times \mathrm{pr}_{\Delta t}(t', t_n)\mathrm{d}t_n, \quad (9)$$

respectively, where $\mathrm{Var}[k_n|t_n]$ in Eq. (9) indicates variance of secondary photons produced by a single primary photon. Applying trigonometric identities to the integrand in Eq. (8) generates dc, ω_p, ω_g, $\Delta\omega_{pg} = \omega_p - \omega_g$, and other high-frequency terms. Except the dc and $\Delta\omega_{p1}$ (i.e., the integer $g = 1$) terms, all other modulation terms are averaged out because the decay time of $p_d^I(t, t_n)$ in Eq. (5) is much larger than modulation periods of these terms. Also, the typical beat frequency for heterodyne measurements is much shorter than $2\pi/\Delta\omega_{p1}$, so $p_d^I(t, t_n) \sim \bar{k}_n^I(t_n)\delta(t - t_n)$ for the dc and $\Delta\omega_{p1}$ terms. With these descriptions, Eq. (8) is simplified to

$$\langle y(t)\rangle \simeq c_p c_0 \int_\infty \left[1 + \frac{m_p m_1}{2} \cos(\Delta\omega_{p1} t_n + \psi)\right] \times \bar{k}_n^I(t_n)\delta(t - t_n)\mathrm{d}t_n = c_p c_0 \bar{k}_n^I \left[1 + \frac{m_p m_1}{2} \cos(\Delta\omega_{p1} t + \psi)\right]. \quad (10)$$

The mean of Eq. (10) is physically reasonable and in agreement with conventionally experienced hetero/homodyne outputs. For the case of homodyne, where $\Delta\omega_{p1} = 0$, the phase difference ψ changes to measure the trajectory of the beat-frequency modulated output. The unit of Eq. (10) is the same as c_p, a photon rate (i.e., units of c_0 and $\bar{k}_n^I$ are photonelectron/primary and secondary/photoelectron, respectively), so multiplying a detector exposure time to Eq. (10) measures the mean output photons.

We define the Fano factor,[18] F, for secondaries per primary as

$$F = \frac{\mathrm{Var}[k_n]}{\bar{k}_n}, \quad (11)$$

which indicates the degree of random amplification of an IIN. It is commonly accepted that F is always greater than 1 in a random amplification process because $F < 1$ means the secondary photons are sub-Poisson for Poisson primaries. Higher F means the amplified output photons are more randomly variable, so measured intensified outputs are less reliable. Considering F of Eq. (11) makes the integrand of $\mathrm{Var}[k_n|t_n]$ in Eq. (9) the same as Eq. (10) with the multiplication of F. The remaining mean square term in Eq. (9) is further developed by substituting Eq. (7) to $\bar{k}_n$. Removing ω_g and higher modulation frequency terms, the integrand of $\bar{k}_n^2(t_n)$ results in

$$c_p(c_0\bar{k}_n^I)^2 \left[1 + \sum_{g=1}^{\infty}\sum_{g'=1}^{\infty} m_g m_{g'} \cos(\omega_g t_n)\cos(\omega_{g'} t_n) + 2m_p \cos(\omega_p t_n + \psi)\sum_{g=1}^{\infty} m_g \cos(\omega_g t_n) + m_p \cos(\omega_p t_n + \psi) \times \sum_{g=1}^{\infty}\sum_{g'=1}^{\infty} m_g m_{g'} \cos(\omega_g t_n)\cos(\omega_{g'} t_n)\right]. \quad (12)$$

Likewise, in the procedure for calculating the mean, only terms containing $\Delta\omega_{p1} = \omega_p - \omega_1$, where $\omega_1 = \omega_g \pm \omega_{g\pm1}$ in Eq. (12), are survived because of the relatively long decay time of $\mathrm{pr}_{\Delta t}(t)$ in Eq. (9). Therefore, the covariance of Eq. (9) becomes

$$K_y \simeq \left\{ \begin{array}{l} c_p c_0 \bar{k}_n^I F\left[1 + \frac{m_p m_1}{2} \cos(\Delta\omega_{p1} t + \psi)\right] \\ + c_p(c_0\bar{k}_n^I)^2 \left[1 + \frac{1}{2}\sum_{g=1}^{\infty} m_g^2 + \frac{m_p}{2}\left(2m_1 + \sum_{\mathrm{odd}\, g} m_g m_{g+1}\right)\cos(\Delta\omega_{p1} t + \psi)\right] \end{array} \right\} \delta(t - t'), \quad (13)$$

where $\mathrm{pr}_{\Delta t}(t, t_n) \sim \delta(t - t_n)$ is applied to Eq. (9). Notice that this Dirac delta function approximation is valid only if the detector integration time ΔT for each measurement point is much longer than the decay time of $\mathrm{pr}_{\Delta t}(t)$. However, ΔT should be much shorter than $2\pi/\Delta\omega_{p1}$ of heterodyne outputs. Therefore, the range of ΔT validating the uncorrelation of the covariance depends on a phosphor of the IIN and a beat frequency of heterodyne outputs. If all m_g are zero, which means non-modulated gain in the IIN, the variance of Eq. (13) becomes the well-known result of the *Burgess Variance theorem*[18,36] for Poisson inputs. For gain modulation as in hetero/homodyne measurements, the covariance of Eq. (13) modulates at the beat frequency $\Delta\omega_{p1}$ like the mean of Eq. (10), where dc (σ_{DC}^2) and ac (σ_{AC}^2) variances can be considered separately. Notice that σ_{DC}^2 in Eq. (13) is increased by the factor of $c_p(c_0\bar{k}_n^I)^2(1/2)\sum_{g=1}^{\infty} m_g^2$, compared with the variance for a non-modulated input ($m_p = 0$), which is the effect of the gain modulation.. Both σ_{DC}^2 and σ_{AC}^2 are strongly dependent on F and $c_0\bar{k}_n^I$, which is an overall dc gain of the IIN, and m_p affects only σ_{AC}^2. Since we discuss mean and variance of output photons, $K_y(t, t')$ is the photon number with the multiplication of ΔT, which is unitless, as the mean.

3 Theory for Spatial Noise Analysis

The mean and covariance of Eqs. (10) and (13) are derived based on the temporal PSF of an IIN, as shown in Eq. (5), where the effect of spatial distribution of the PSF is omitted. The temporal

consideration would be valid for photoelectrons from a MCP output pore because photoelectrons incident into each MCP input pore are Poisson and MCP channels are physically separated from each other. As shown in Fig. 1(a), however, secondaries from a single MCP output pore are spatially distributed to multiple CCD pixels, which should be considered for the noise analysis of photons detected on a CCD. It is reasonable to assume that the event of detecting one photon among secondaries from a specific MCP output pore by a certain CCD pixel does not affect other secondary photons from the MCP output pore. With this assumption, the spatial distribution of secondaries is theoretically described by a multinomial selection rule.[18]

To simplify the mathematics, simplified terminologies are used for the spatial noise analysis. If the number of total photons detected by the α'th CCD pixel during some measurement time T is M_α,

$$M_\alpha = \sum_i m_{\alpha i}, \tag{14}$$

where $m_{\alpha i}$ indicates the number of photons detected on the α'th CCD pixel from i'th MCP output pore. The summation in Eq. (14) is for all MCP output pores contributing to M_α. Like the temporal noise analysis, T is assumed to be much longer than an anode decay time in the IIN. The mean $\langle M_\alpha \rangle$ is derived as

$$\begin{aligned}\langle M_\alpha \rangle &= \sum_i \sum_{m_{\alpha i}=0}^{\infty} m_{\alpha i} \Pr(m_{\alpha i}) \\ &= \sum_i \sum_{m_{\alpha i}=0}^{\infty} \sum_{K_i=m_{\alpha i}}^{\infty} m_{\alpha i} \Pr(m_{\alpha i}|K_i) \Pr(K_i) \\ &= \sum_i P_{\alpha i} \bar{K}_i, \end{aligned} \tag{15}$$

where $P_{\alpha i}$ is the probability that photons from i'th MCP pore are detected on α'th CCD pixel and $\bar{K}^I$ indicates mean total photons from the i'th MCP pore. In the procedure of Eq. (15), averaging is done for two random variables $m_{\alpha i}$ and K_i with a multinomial PDF $\Pr(m_{\alpha i}|K_i)$ and $\Pr(K_i)$ that is unknown, respectively. For convenience, these two averages are denoted as $\langle\rangle_m$ and $\langle\rangle_K$ to calculate the covariance $C[M_\alpha, M_\beta] = \langle M_\alpha M_\beta \rangle - \langle M_\alpha \rangle \langle M_\beta \rangle$. The second moment of $\langle M_\alpha M_\beta \rangle$ is

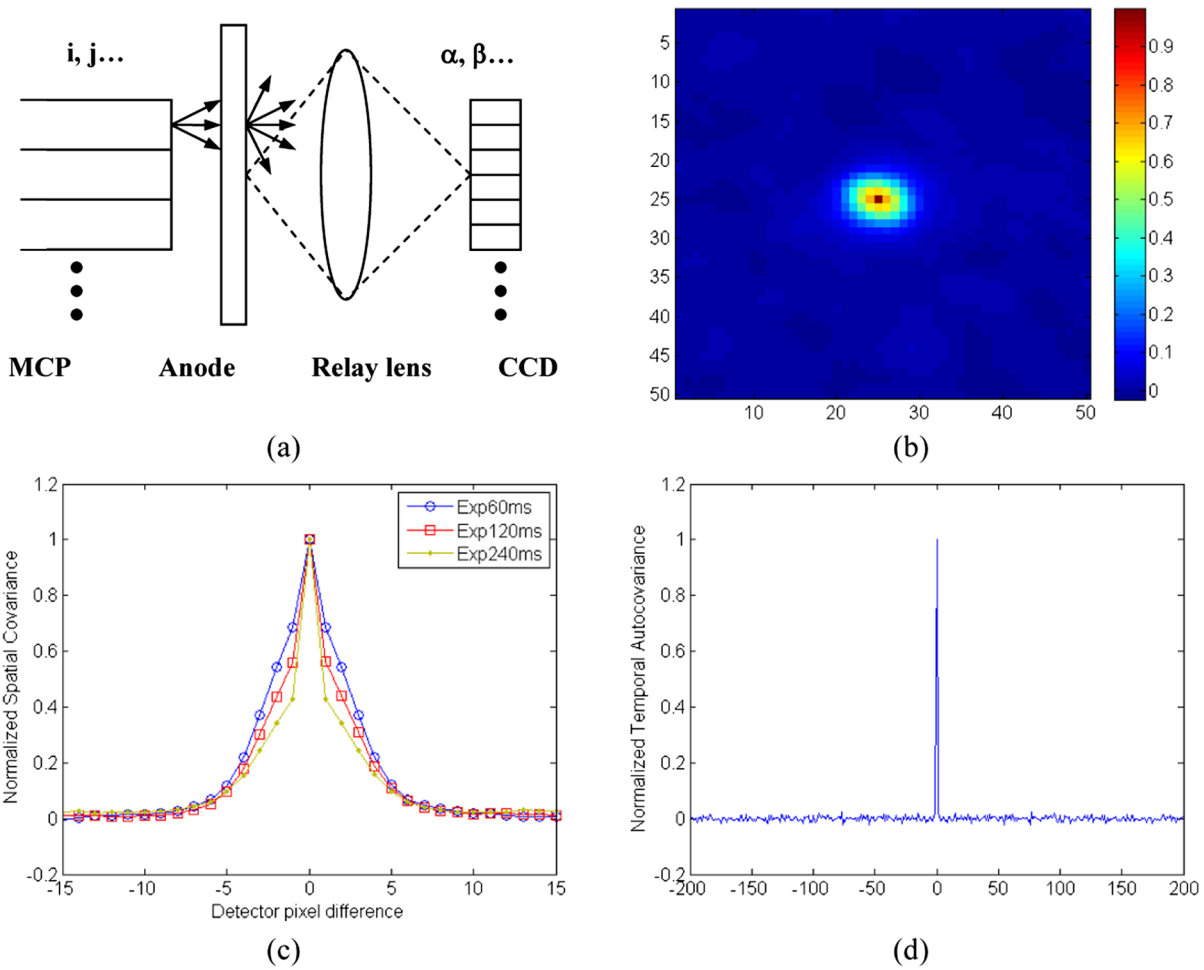

Fig. 1 (a) Simple scheme for the spatial distribution of secondary photons. Experimentally measured profiles [(b) 2-D and (c) 1-D] of averaged normalized spatial covariance. In (c), circles, squares, and dots indicate exposure times of 60, 120, and 240 ms, respectively. In (d), the temporal autocovariance measured at a single CCD pixel is indicated.

$$\langle M_\alpha M_\beta \rangle = \sum_{i,j} \langle m_{\alpha i} m_{\beta j} \rangle_{m,K} = \sum_{i \neq j} P_{\alpha i} P_{\beta j} \langle K_i K_j \rangle_K + \sum_{i=j} \langle P_{\alpha i} K_i \delta_{\alpha\beta} - P_{\alpha i} P_{\beta i} K_i + P_{\alpha i} P_{\beta i} K_i^2 \rangle_K, \quad (16)$$

where the covariance of a multinomial PDF is applied to the second step and $\delta_{\alpha\beta}$ is 1 only if $\alpha = \beta$, otherwise 0. Because a multinomial selection of Poisson results in Poisson,[18] photoelectrons incident into each MCP input pore are also Poisson, which indicates that $\langle K_i K_j \rangle_K$ in Eq. (16) can be approximated to $\bar{K}_i \bar{K}_j$. Then, from Eq. (16), the covariance is

$$C[M_\alpha, M_\beta] = \sum_i [P_{\alpha i} \bar{K}_i \delta_{\alpha\beta} + P_{\alpha i} P_{\beta i} (\sigma_{K_i}^2 - \bar{K}_i)], \quad (17)$$

where $\langle K_i^2 \rangle_K = \sigma_{K_i}^2 + (\bar{K}_i)^2$ is used in the second term of Eq. (16) to derive Eq. (17). The variance of photons detected on a single CCD pixel (i.e., α'th pixel) is given by $\alpha = \beta$ in Eq. (17). $C[M_\alpha, M_\beta]$ of Eq. (17) shows that measured images on a CCD from an IIN are spatially correlated and the correlation length is mainly determined by $P_{\alpha i}$. It is known that the efficiency of a photon transferring from an anode to a CCD in a typical IIN having a relay lens imaging system is $10 \sim 15\%$. Therefore, the first term in Eq. (17) cannot be ignorable for the variance, unless $\sigma_{K_i}^2$ is much higher than $\bar{K}_i$. We insist that the spatial noise property shown in Eq. (17) is general in IINs and should be considered even for a PMT. In a PMT, only two probabilities of detected and lost photons are considered, so $P_{\alpha i}$ might be much higher than that in IINs. Moran et al.[28] analyzed a spatial noise property in ICCDs by introducing a spatiotemporal PSF, but their procedure is very complicated and their result is different from Eq. (17). Experimental results showing the covariance of Eq. (17) in IIN outputs are presented in the next section.

Complete noise expressions of hetero/homodyne measurements are given by combining the temporal and spatial analyses. Resulting from this, dc and ac means and variances on α'th CCD pixel in the frequency-domain measurement are

$$\bar{M}_{\mathrm{DC}} = c_p \sum_i P_{\alpha i} (c_0 \bar{k}_n^I)_i,$$

$$\bar{M}_{\mathrm{AC}} = \frac{c_p m_p}{2} \sum_i P_{\alpha i} (c_0 \bar{k}_n^I m_1)_i,$$

$$\sigma_{\mathrm{DC}}^2 = c_p \left\{ \sum_i P_{\alpha i} (c_0 \bar{k}_n^I)_i + \sum_i P_{\alpha i}^2 \left[c_0 \bar{k}_n^I (F-1) + (c_0 \bar{k}_n^I)^2 \left(1 + \frac{1}{2} \sum_{g=1}^{\infty} m_g^2 \right) \right]_i \right\},$$

and

$$\sigma_{\mathrm{AC}}^2 = \frac{c_p m_p}{2} \left\{ \sum_i P_{\alpha i} (c_0 \bar{k}_n^I m_1)_i + \sum_i P_{\alpha i}^2 \left[c_0 \bar{k}_n^I m_1 (F-1) + (c_0 \bar{k}_n^I)^2 \left(2m_1 + \sum_{\text{odd } g} m_g m_{g+1} \right) \right]_i \right\}, \quad (18)$$

respectively. For Eq. (18), we assumed that c_p and m_p of modulated output photons from a phantom slowly vary across the phantom exit surface or the cathode of the IIN, so these quantities are almost the same for each MCP channel contributing to the noise property of photons detected at α'th CCD pixel. This assumption is reasonable because the degree of diffusion (i.e., scattering) of tissues in medical imaging is usually large. It is important that both mean and variance modulate along $\cos(\Delta\omega_{p1} t + \psi)$ with these dc and ac means and variances in Eq. (18). Equation (18) also shows that $\bar{M}_{\mathrm{AC}}$ and σ_{AC}^2 are approximately different from $\bar{M}_{\mathrm{DC}}$ and σ_{DC}^2, respectively, by the factor of $m_p m_1/2$. When the gain of the IIN increases, both F and $c_0 \bar{k}_n^I$ are increased, which indicates that the second terms of $P_{\alpha i}^2$ in both dc and ac variances are significant. It is expected that although σ_{DC}^2 and σ_{AC}^2 are increased as increasing the gain, the relative difference between these two variances becomes larger because the multiplication factor $m_p m_1/2$ in σ_{AC}^2 is typically less than 1. Furthermore, Eq. (18) implies that as the modulation gain of the IIN deviates from a perfect sinusoidal function more and more, the noise of the hetero/homodyne is increased more due to higher values for $m_g s$.

4 Experiment

The CCD and the IIN used in the experiment are Point Grey F2-08S2M and Lambert Ins. II18MD, respectively. The source is the laser diode (LDH-M-C-650B) from PicoQuant with the modulated diode laser driver, MDL 300. This driver is run by external modulation signals from a Tektronix AFG3252 function generator that also generates modulation signals for the IIN cathode. The CCD is carefully adjusted onto the image plane of the relay lens of the IIN in Fig. 1(a) before the main experiment. Since the experiment of measuring variances usually takes a few hours, the experiment starts after about 2 h of warming-up to thermally stabilize all instruments. Especially, voltages directly measured from the cathode of the IIN show that the cathode is thermally unstable at the initial run, which might cause an unexpected long-term variation during the measurement. The laser diode (LD) beam incident into the IIN is almost spatially flat and speckle-free in intensity, which is achieved by lenses and ground glasses. Also, neutral density filters are used to decrease the power of the LD to avoid damage to the IIN cathode, because harmonic distortions of the modulated LD beam can be minimized by keeping the LD power high.

Figure 1(b) is the averaged variance-normalized spatial covariance calculated from images for non-modulated incident beams to the IIN with a non-modulated gain. The averaging is done with 49 variance-normalized spatial covariance matrices, where each of them is normalized by its own variance. The exposure time T is 60 ms, and 2000 images are captured to calculate the spatial covariance. The transverse magnification of the relay lens in the IIN is 0.5 and the CCD pixel size is $7.4 \times 7.4\ \mu\mathrm{m}^2$, so the pixel size on the anode surface in Fig. 1(b) is equivalent to $\sim 14.8 \times 14.8\ \mu\mathrm{m}^2$. As shown in Fig. 1(b), the data are spatially correlated, which is caused by the secondary photon distribution from MCP output pores to CCD pixels. Figure 1(c) shows 1-D profiles of calculated spatial covariance matrices for different MCP voltages. The exposure time T is adjusted for different MCP voltages so that measured means are almost the same, where Exp60 ms in the legend indicates 60 ms CCD exposure time and highest MCP voltage. As the MCP voltage gets higher (i.e., the IIN gain is higher), the variance becomes larger than the mean for a single MCP output pore, so the contribution of the second term of

Eq. (17) to the variance for a CCD pixel is also increased. This is the reason that the width of variance-normalized correlation functions is decreased with decreasing MCP voltage, as shown in Fig. 1(c). It is noticed that the correlation length is almost the same for all three MCP voltages, which indicates that $P_{\alpha i}$ in Eq. (17) is almost independent of a MCP voltage. We observed that even modulating the cathode voltage does not have a large affect on these correlation functions. Figure 1(d) is a variance-normalized temporal auto covariance from data measured at a single CCD pixel for $T = 60$ ms. Since 60 ms of T is much longer than the decay time of the phosphor (1 ms to drop 1% of the peak output for P43 in II18MD), data are temporally uncorrelated as expected. The experimental results in Fig. 1 show that the approach of a multinomial PDF for the spatial distribution of secondaries is reasonable and that its effect can be independently considered from the temporal point process analysis.

A homodyne method is used to experimentally measure σ^2_{DC} and σ^2_{AC} of Eq. (18), because it is more appropriate for measuring multiple images than a heterodyne method. Applying a high modulation frequency to the cathode in the IIN for a long time could permanently damage the cathode, so the modulation frequency for this experiment is set to 100 kHz. Although 100 kHz is several hundred times lower than a typical modulation frequency used in frequency-domain diffusive imaging, the noise characteristics shown in Eq. (18) can still be observed. Also, 4×4 CCD pixels are considered a single macro pixel, which increases the reliability of measuring variances without dramatically increasing the number of images, hence reducing the overall measurement time. As the first step, a homodyne profile is measured with 64 phase steps for 2π of the phase difference (ψ) between modulation signals applied to the IIN and LD. Homodyne profiles measured at three observer points (ObPs) of a macro pixel are shown in Fig. 2(a), indicating that these profiles are slightly different for different macro pixels. The maximum detector output (bin) is $2^{12} = 4096$. Each measurement point in these homodyne profiles is produced by averaging 50 homodyne images. Next, the averaged homodyne profile is calculated from 100 homodyne profiles measured at different macro pixels within an arbitrarily chosen local detector area. From this averaged homodyne profile, three ψ's corresponding to maximum, dc, and minimum irradiances of the homodyne profile are sought. After these ψ's are found, 1000 images are measured for each ψ to calculate means ($\bar{M}_{\mathrm{min}}$, $\bar{M}_{\mathrm{DC}}$, $\bar{M}_{\mathrm{max}}$) and variances (σ^2_{min}, σ^2_{DC}, σ^2_{max}) for all 100 macro pixels within the arbitrarily chosen local detector area. Finally, $\bar{M}_{\mathrm{AC}}$ and σ^2_{AC} are calculated from $1/2(\bar{M}_{\mathrm{max}} - \bar{M}_{\mathrm{min}})$ and $1/2(\sigma^2_{\mathrm{max}} - \sigma^2_{\mathrm{min}})$, respectively. Macro pixels satisfying the ac

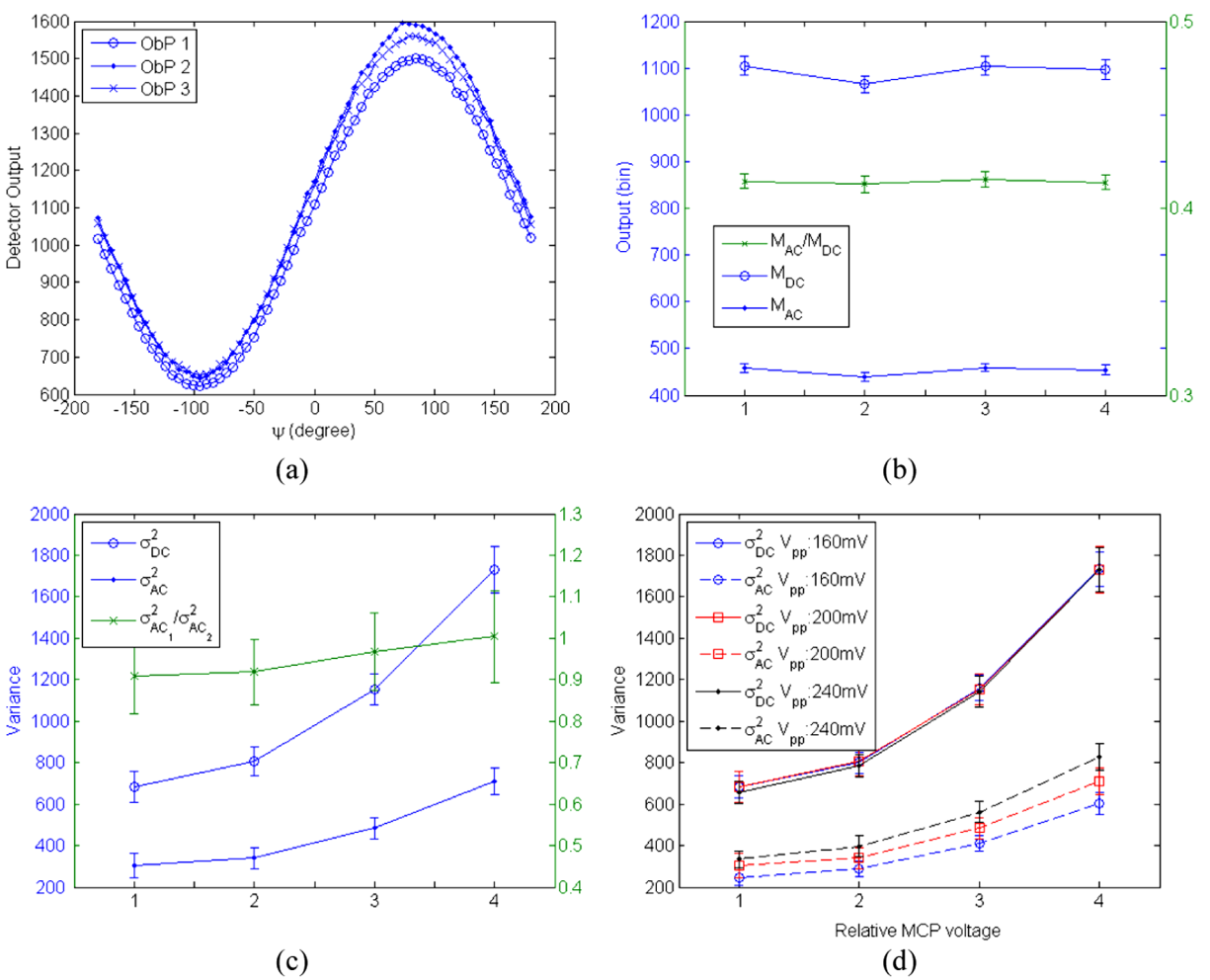

Fig. 2 (a) Examples of measured homodyne profile. (b) Means and (c) variances of measured dc and ac. Labels on right y-axes in (b) and (c) indicate ratios of $\bar{M}_{\mathrm{AC}}/\bar{M}_{\mathrm{DC}}$ and $\sigma^2_{\mathrm{AC1}}/\sigma^2_{\mathrm{AC2}}$, respectively. (d) Varied m_p changes not dc variance, but ac variance of homodyne outputs. The x-axes for (b) and (c) indicate relative MCP voltages.

mean ratio of $\bar{M}_{\max} - \bar{M}_{DC}$ and $\bar{M}_{DC} - \bar{M}_{\min}$ is almost 1 are selected for investigating noise characteristics of Eq. (18), the number of which is ~30 out of 100. Macro pixels showing ac mean ratios not close to 1 indicate that their homodyne profiles deviate much from the averaged homodyne profile.

Figure 2(b) shows measured $\bar{M}_{DC}$, $\bar{M}_{AC}$ and their ratios to different MCP voltages that are indicated as numbers in the x-axis. T for these different MCP voltages are set to 60, 120, 240, and 480 ms. The MCP voltages for these T's are chosen to make all measured $\bar{M}_{DC}$ the same, where 1 MCP voltage in Fig. 2 corresponds to $T = 60$ ms. The primary photon number Tc_p increases as T is increased, but it can be considered that primary photons are still Poisson for even $T = 480$ ms due to a very small output photon rate incident into the IIN. If m_p and m_1 are assumed almost constant within each measurement macro pixel, $\bar{M}_{AC}/\bar{M}_{DC} \sim m_p m_1/2$ from Eq. (18). Since the separately measured m_p in this experimental setup is ~0.6, and $\bar{M}_{AC}/\bar{M}_{DC} \sim 0.415$ in Fig. 2(b), which indicates that m_1 of the cathode modulation is ~1.37. We observed that measured values of $\bar{M}_{AC}/\bar{M}_{DC}$ are around $0.39 \sim 0.42$ for all conducted experiments as long as applied modulation voltages to the cathode of IIN and LD remain the same. The different values of $\bar{M}_{AC}/\bar{M}_{DC}$ indicate that the characteristics of gain modulation are slightly different, macro pixel by pixel. Measured σ^2_{DC}, σ^2_{AC} and $\sigma^2_{AC1}/\sigma^2_{AC2}$ to different MCP voltages are shown in Fig. 2(c), where $\sigma^2_{AC1} = \sigma^2_{\max} - \sigma^2_{DC}$ and $\sigma^2_{AC2} = \sigma^2_{DC} - \sigma^2_{\min}$. The value $\sigma^2_{AC1}/\sigma^2_{AC2} \sim 1$ indicates the validity of the experiment. Figure 2(c) shows that both σ^2_{DC} and σ^2_{AC} increase as the MCP voltage increases, although $\bar{M}_{DC}$ and $\bar{M}_{AC}$ are constant as in Fig. 2(b). This means that F and $\bar{k}^I_n$ in Eq. (18) dramatically increase as the MCP voltage (i.e., gain of the IIN) increases. From the other view, it is observed that the decreasing rates of both σ^2_{DC} and σ^2_{AC} are smaller for a lower MCP voltage, which indicates the mean terms contributing to variances in Eq. (18) are more dominant. It is also observed in Fig. 2(c) that the absolute difference between σ^2_{DC} and σ^2_{AC} is increased as the MCP voltage increases, which is caused by $m_p m_1/2 \sim 0.415$ in σ^2_{AC} of Eq. (18). Since the developed theory in Eq. (18) shows that m_p affects not σ^2_{DC} but σ^2_{AC}, we measure the variation of variances with different peak-to-peak voltages (V_{pp}) of the modulation signal applied to LD, which changes m_p. As shown in Fig. 2(d), σ^2_{DC}'s are almost invariant to V_{pp}, but σ^2_{AC}'s are proportionally changed to V_{pp}. As shown in Fig. 2, experimental results show good agreement with the developed theory of Eq. (18).

5 Discussion and Conclusion

A noise factor, NF, is commonly used for the study of noise properties in photon amplifiers, such as ICCDs or IINs.[28] Although the noise factor NF is defined for the case of non-modulation gain in photon amplifiers, it is worth making a relationship between NF and F for applying NF to Eq. (18), which is

$$NF \equiv \frac{\mathrm{SNR}_i^2}{\mathrm{SNR}_o^2} = \frac{m_i \sigma_o^2}{m_o^2} = \frac{F}{c_0 \bar{k}^I_n}, \tag{19}$$

where the subscripts i and o indicate input and output, and m_i and m_o are means of primary and secondary photons, respectively. It is assumed that the primary photons are Poisson in the second step and $m_i c_0 \bar{k}^I_n = m_o$ is applied to the third step of Eq. (19). Substituting Eq. (19) to Eq. (18) can express σ^2_{DC} and σ^2_{AC}, including NF. For example, σ^2_{DC} becomes

$$\sigma^2_{DC} \simeq c_p \left\{ \sum_i P_{\alpha i} (c_0 \bar{k}^I_n)_i + \sum_i P^2_{\alpha i} (c_0 \bar{k}^I_n)^2_i \left[NF + 1 + \frac{1}{2} \sum_{g=1}^{\infty} m_g^2 \right]_i \right\}, \tag{20}$$

where $1/c_0 \bar{k}^I_n$ in the second term of Eq. (20) is ignored assuming $c_0 \bar{k}^I_n \gg 1$. It is reported that a NF for MCP outputs in an ICCD is inversely proportional to the MCP voltage.[28] From the experimental results in Fig. 2 and Eq. (20), it can be conjectured that $(c_0 \bar{k}^I_n)[NF + 1 + \frac{1}{2}\sum_{g=1}^{\infty} m_g^2]$ is dramatically increased as the MCP voltage increases even though a NF is decreased. A similar phenomenon is experimentally observed in other study, where $c_0 \bar{k}^I_n NF$ is increased as a MCP voltage increases although NF is decreased.[28] As another issue, characterizing the noise property of photon amplifiers by measuring a NF as a function of gain should be done carefully. As shown in Eq. (20), the NF for MCP output photons might be significantly different from the NF for amplifiers' outputs depending on the amount of $P_{\alpha i}$ when $c_0 \bar{k}^I_n$ is low.

The noise model of hetero/homodyne outputs is theoretically derived considering random amplification and multinomial selection. The noise characteristics determined from the developed theory are experimentally verified. Although this noise model is developed for hetero/homodyne measurements in this paper, it can be used for the case of non-modulation input beam and gain. Furthermore, it is reasonable to assume that the primary photons for most amplification processes are described by Poisson point process, as assumed in this paper. Therefore, the model in this paper can be applied to most photon-amplification processes including PMTs and Avalanche photodiodes (APDs) with or without gain modulation.

Some valuable properties are obtained from the developed noise model. The output is temporally uncorrelated, like shot noise, only if detector integration time for sampling is much longer than the decay time of phosphors in imaging intensifiers. For heterodyne measurements, the exposure time should be much less than the period of beat-frequency heterodyne output. Therefore, the heterodyne output is temporally uncorrelated for the specific range of the detector integration time. The amount of variance oscillates like the heterodyne and/or homodyne mean, so dc and ac variances can be considered separately. The dc variance indicates that the noise of the frequency-domain measurement output is amplified by the random amplification and gain modulation compared with the case of non-modulation gain. As the gain modulation deviates more from a perfect sinusoidal function, both dc and ac variances are increased. Another interesting point is that when both the gain of the image intensifier and the probability of detecting amplified photons from the image intensifier on a detector pixel are low, the variance approaches the mean—that is, the output photons are close to Poisson.

Hetero/homodyne measurements are widely used in frequency-domain diffusive imaging, so understanding the noise property of the frequency-domain outputs is beneficial in many ways. For example, it has recently been reported that estimated means of modulation amplitude and phase from noisy hetero/homodyne outputs are biased when the number of output

photons is small.[37] By adapting the expressions of mean and covariance developed in this paper, we have practically clarified the relationship between the bias and primary photon number. Furthermore, the developed noise model would be useful to precisely estimate modulation amplitude and phase using a maximum likelihood estimation method. As another example, the noise model in this paper could consolidate figures of merit for evaluating diffusive imaging performance, which is effective at optimizing frequency-domain diffusive imaging systems and helpful in developing new modalities of them. Finally, the performance of reconstruction algorithms can be enhanced with the appropriate noise model, so the theoretical results in this paper can be adapted to improve the quality of reconstructed images from frequency-domain tomographic diffusive imaging.

Appendix:

For the mean of Eq. (1), averaging for Δt_{nk} is

$$\begin{aligned}\langle y(t)\rangle_{\{\Delta t_{nk}\}} &= \sum_{n=1}^{N}\sum_{k=1}^{k_n}\int_{\infty}\delta(t-t_n-\Delta t_{nk})[\bar{k}_n(t_n)]^{-1} \\ &\quad\times p_d(\Delta t_{nk}+t_n,t_n)\Delta t_{nk} \\ &= \sum_{n=1}^{N}\sum_{k=1}^{k_n}[\bar{k}_n(t_n)]^{-1}p_d(t,t_n) \\ &= \sum_{n=1}^{N}k_n[\bar{k}_n(t_n)]^{-1}p_d(t,t_n),\end{aligned} \tag{21}$$

where the marginal probability for all $\Delta t_{n'k'}$ except $n'=n$ and $k'=k$ for any particular n and k are conducted on the first line []. The last step in Eq. (21) is done by that $[\bar{k}_n(t_n)]^{-1}$ is independent of k. The averaging for the secondary k_n simply replaces k_n in Eq. (21) to $\bar{k}_n(t_n)$, so

$$\langle y(t)\rangle_{\{\Delta t_{nk}\},\{k_n\}} = \sum_{n=1}^{N}p_d(t,t_n). \tag{22}$$

From Eq. (3), the averaging for secondary time t_n produces

$$\langle y(t)\rangle_{\{\Delta t_{nk}\},\{k_n\},\{t_n\}} = \sum_{n=1}^{N}[N(a_p)]^{-1}\int_{\infty}p_d(t,t_n)a_p(t_n)\mathrm{d}t_n. \tag{23}$$

With the similar concept of independence conducted from Eqs. (21) to (22), further averaging Eq. (23) with N becomes

$$\langle y(t)\rangle_{\{\Delta t_{nk}\},\{k_n\},\{t_n\},\{N\}} = \int_{\infty}p_d(t,t_n)a_p(t_n)\mathrm{d}t_n. \tag{24}$$

Substituting Eqs. (2) and (5) to Eq. (24) finalizes the calculation for the mean, as shown in Eq. (8).

The covariance can be calculated with the similar averaging procedure from Eqs. (21)–(26), but it should be considered in three separate cases. The autocorrelation of the point process of Eq. (1) is expressed as

$$R_y(t,t') = \left\langle\sum_{n=1}^{N}\sum_{k=1}^{k_n}\sum_{n'=1}^{N}\sum_{k=1}^{k_{n'}}\delta(t-t_n-\Delta t_{nk})\delta(t'-t_{n'}-\Delta t_{n'k'})\right\rangle. \tag{25}$$

Case 1: $n=n'$, $k=k'$

The averaging over Δt_{nk} for the autocorrelation with the condition of case 1 is

$$\langle y(t)y(t')\rangle^{(1)}_{\{\Delta t_{nk}\}} = \sum_{n=1}^{N}\sum_{k=1}^{k_n}[\bar{k}_n(t_n)]^{-1}p_d(t,t_n)\delta(t-t'), \tag{26}$$

where a marginal probability law for Δt_{nk} is similarly applied, as in Eq. (21). The superscript (1) indicates that averaging is performed for case 1. Further averaging Eq. (26) for k_n, t_n, and N produces

$$R_y^{(1)}(t,t') = \int_{\infty}p_d(t,t_n)a_p(t_n)\mathrm{d}t_n\delta(t-t'). \tag{27}$$

Substituting Eqs. (2) and (5) to Eq. (27) derives

$$\begin{aligned}R_y^{(1)}(t,t') &= c_pc_0\int_{\infty}[1+m_p\cos(\omega_pt_n+\psi)] \\ &\quad\times\left[1+\sum_{g=1}^{\infty}m_g\cos(\omega_gt_n+\phi_s)\right] \\ &\quad\times p_d^I(t,t_n)\mathrm{d}t_n\delta(t-t').\end{aligned} \tag{28}$$

Similar with the procedure from Eqs. (8)–(10), only the dc and $\Delta\omega_{p1}$ terms survive in Eq. (28). Therefore,

$$\begin{aligned}R_y^{(1)}(t,t') &= c_pc_0\bar{k}_n^I\left[1+\frac{m_p}{2}\cos(\Delta\omega_{p1}t+\psi-\phi_1)\sum_{g=1}^{\infty}m_g\right] \\ &\quad\times\delta(t-t'),\end{aligned} \tag{29}$$

where it is assumed that $p_d^I(t,t_n)\approx\bar{k}_n^I(t_n)\delta(t-t_n)$.

Case 2: $n=n'$, $k\neq k'$.

Considering a marginal probability law, averaging Eq. (25) over Δt_{nk} produces

$$\begin{aligned}\langle y(t)y(t')\rangle^{(2)}_{\{\Delta t_{nk}\}} &= \sum_{n=1}^{N}\sum_{k=1}^{k_n}\sum_{k'=1}^{k_n}\int_{\infty}\int_{\infty}p_{\Delta t}(\Delta t_{nk},\Delta t_{nk'}) \\ &\quad\times\delta(t-t_n-\Delta t_{nk})\delta(t'-t_n-\Delta t_{nk'})d\Delta t_{nk}d\Delta t_{nk'} \\ &= \sum_{n=1}^{N}\sum_{k=1}^{k_n}\sum_{k'=1}^{k_n}[\bar{k}_n(t_n)]^{-2}p_d(t,t_n)p_d(t',t_n) \\ &= \sum_{n=1}^{N}(k_n^2-k_n)[\bar{k}_n(t_n)]^{-2}p_d(t,t_n)p_d(t',t_n),\end{aligned} \tag{30}$$

where the second line is given by that Δt_{nk} and $\Delta t_{n'k'}$ are independent of each other. The $k_n^2-k_n$ indicates the number of terms on the summations of k and k' for $k\neq k'$, which can

be switched to $\mathrm{Var}[k_n|t_n] + \bar{k}_n^2(t_n) - \bar{k}_n(t_n)$ through the procedure of averaging Eq. (30) over k_n. Further averaging $\langle y(t)y(t')\rangle^{(2)}$ for t_n and N becomes

$$R_g^{(2)}(t,t') = \int_\infty [\mathrm{Var}[k_n|t_n] + \bar{k}_n^2(t_n) - \bar{k}_n(t_n)][\bar{k}_n(t_n)]^{-2} \times a_p(t_n)p_d(t,t_n)p_d(t',t_n)\mathrm{d}t_n. \quad (31)$$

If the integration for the term $\bar{k}_n(t_n)$ in $[\mathrm{Var}[k_n|t_n] + \bar{k}_n^2(t_n) - \bar{k}_n(t_n)]$ is considered with the substitutions of Eqs. (2), (5), and (7),

$$\begin{aligned}
&\int_\infty [\bar{k}_n(t_n)]^{-1}p_d(t,t_n)p_d(t',t_n)a_p(t_n)\mathrm{d}t_n \\
&= c_p c_0 \int_\infty [\bar{k}_n^I(t_n)]^{-1}p_d^I(t,t_n)p_d^I(t',t_n)[1+m_p \\
&\quad \times \cos(\omega_p t_n + \psi)]\left[1 + \sum_{g=1}^{\infty} m_g \cos(\omega_g t_n + \phi_g)\right]\mathrm{d}t_n \\
&\approx c_p c_0 \int_\infty \bar{k}_n^I(t_n)\delta(t-t_n)\delta(t'-t_n) \\
&\quad \times \left[1 + \frac{m_p}{2}\cos(\Delta\omega_{p1}t + \psi - \phi_1)\sum_{g=1}^{\infty} m_g\right]\mathrm{d}t_n \\
&\approx c_p c_0 \bar{k}_n^I\left[1 + \frac{m_p}{2}\cos(\Delta\omega_{p1}t + \psi - \phi_1)\sum_{g=1}^{\infty} m_g\right]\delta(t-t).
\end{aligned} \quad (32)$$

The last line of Eq. (32) is equivalent to Eq. (29), so these are canceled out for the autocorrelation considering both case 1 and case 2. The autocorrelation is

$$R_y^{(1)+(2)}(t,t') = \int_\infty [\mathrm{Var}[k_n|t_n] + \bar{k}_n^2(t_n)]a_p(t_n)\mathrm{pr}_{\Delta t}(t,t_n)\mathrm{pr}_{\Delta t}(t',t_n)\mathrm{d}t_n, \quad (33)$$

where Eq. (6) is used for p_d in Eq. (31).

Case 3: $n \neq n'$, $k \neq k'$.

Calculating the autocorrelation under this condition is so straightforward that the detailed mathematical procedure is not shown. Basically, after considering that there are $N^2 - N$ terms for the summations for n and n', two point processes $g(t)$ and $g(t')$ can be independently calculated. Resulting from this consideration is the multiplication of two means of Eq. (24). Because the covariance $K_y(t,t') = R_y(t,t') - \langle y(t)\rangle\langle y(t')\rangle$, the result $R_y(t,t')$ of for case 3 is canceled out with $\langle y(t)\rangle\langle y(t')\rangle$ in $K_y(t,t')$. Therefore, $K_y(t,t')$ is the same as Eq. (31), which is the same as Eq. (9).

References

1. A. P. Gibson, J. C. Hebden, and S. R. Arridge, "Recent advances in diffuse optical imaging,," *Phys. Med. Biol.* **50**, R1–R43 (2005).
2. D. A. Boas et al., "Imaging the body with diffuse optical tomography," *IEEE Signal Process. Mag.* **1053**, 57–75 (2001).
3. U. J. Netz, J. Beuthan, and A. H. Hielscher, "Multipixel system for gigahertz frequency-domain optical imaging of finger joints," *Rev. Sci. Instrum.* **79**(3), 034301 (2008).
4. Z. M. Wang et al., "Experimental demonstration of an analytic method for image reconstruction in optical diffusion tomography with large data sets," *Opt. Lett.* **30**(24), 3338–3340 (2005).
5. G. Y. Panasyuk et al., "Fluorescent optical tomography with large data sets," *Opt. Lett.* **33**(15), 1744–1746 (2008).
6. B. Chance et al., "Phase measurement of light absorption and scatter in human tissue," *Rev. Sci. Instrum.* **69**(10), 3457–3481 (1998).
7. A. B. Thompson and E. M. Sevick-Murace, "Near-infrared fluorescence contrast-enhanced imaging with intensified charge-coupled device homodyne detection: measurement precision and accuracy," *J. Biomed. Opt.* **8**(1), 111–120 (2003).
8. S. R. Arridge and W. R. Lionheart, "Nonuniqueness in diffusion-based optical tomography," *Opt. Lett.* **23**(11), 882–884 (1998).
9. G. Xu et al., "Direct-current-based image reconstruction versus direct-current included or excluded frequency-domain reconstruction in diffuse optical tomography," *Appl. Opt.* **49**(16), 3059–3070 (2010).
10. J. R. Lakowicz et al., "Fluorescence lifetime imaging," *Anal. Biochem.* **202**, 316–330 (1992).
11. E. Gratton et al., "Fluorescence lifetime imaging for the two-photon microscope: time-domain and frequency-domain methods," *J. Biomed. Opt.* **8**(3), 381–390 (2003).
12. A. Esposito, H. C. Gerritsen, and F. S. Wouters, "Optimizing frequency-domain fluorescence lifetime sensing for high-throughput applications: photon economy and acquisition speed," *J. Opt. Soc. Am. A* **24**(10), 3261–3273 (2007).
13. A. Elder, S. Schlachter, and C. F. Kaminski, "Theoretical investigation of the photon efficiency in frequency-domain fluorescence lifetime imaging microscopy," *J. Opt. Soc. Am. A* **25**(2), 452–462 (2008).
14. D. Y. Paithankar et al., "Imaging of fluorescent yield and lifetime from multiply scattered light reemitted from random media," *Appl. Opt.* **36**(10), 2260–2272 (1997).
15. A. R. Pineda et al., "Information content of data types in time-domain optical tomography," *J. Opt. Soc. Am. A* **23**(12), 2989–2996 (2006).
16. H. K. Kim et al., "Optimal source-modulation frequencies for transport-theory-based optical tomography of small-tissue volumes," *Opt. Express* **16**(22), 18082–18101 (2008).
17. T. Tu et al., "Analysis on performance and optimization of frequency-domain near-infrared instruments," *J. Biomed. Opt.* **7**(4), 643–649 (2002).
18. H. H. Barrett and K. J. Myers, *Foundations of Image Science*: Wiley, New York (2004).
19. H. H. Barrett et al., "Objective assessment of image quality. II. Fisher information, Fourier crosstalk, and figures of merit for task performance," *J. Opt. Soc. Am. A* **12**(5), 834–852 (1995).
20. J. Y. Hesterman et al., "Hardware assessment using the multi-module, multi-resolution system (M^3R): a signal-detection study," *Med. Phys.* **34**(7), 3034–3044 (2007).
21. H. H. Barrett, "Objective assessment of image quality: effects of quantum noise and object variability," *J. Opt. Soc. Am. A* **7**(7), 1266–1278 (1990).
22. C. K. Abbey and H. H. Barrett, "Human- and model-observer performance in ramp-spectrum noise: effects of regularization and object variability," *J. Opt. Soc. Am. A* **18**(3), 473–488 (2001).
23. V. Toronov et al., "Optimization of the signal-to-noise ratio of frequency-domain instrumentation for near-infrared spectro-imaging of the human brain," *Opt. Express* **11**(21), 2717–2729 (2003).
24. S. P. Morgan, "Detection performance of a diffusive wave phased array," *Appl. Opt.* **43**(10), 2071–2078 (2004).
25. D. Kang and M. A. Kupinski, "Signal detectability in diffusive media using phased arrays in conjunction with detector arrays," *Opt. Express* **19**(13), 12261–12274 (2011).
26. J. Philip and K. Carlsson, "Theoretical investigation of the signal-to-noise ratio in fluorescence lifetime imaging," *J. Opt. Soc. Am. A* **20**(2), 368–379 (2003).
27. R. L. Bell, "Noise figure of the MCP image intensifier tube," *IEEE Trans. Electron. Dev.* **22**(10), 821–829 (1975).
28. S. E. Moran et al., "Intensified CCD (ICCD) dynamic range and noise performance," *Proc. SPIE* **3173**, 430–457 (1997).
29. J. McGinty et al., "Signal-to-noise characterization of time-gated intensifiers used for wide-field time-domain FLIM," *J. Phys. D: Appl. Phys.* **42**, 135103 (2009).

30. V. V. Apanasovich and E. G. Novikov, "Mathematical model of the microchannel plate single electron impulse formation," *IEEE Trans. Electron. Dev.* **42**(21), 2231–2235 (1995).
31. A. Frenkel, M. A. Sartor, and M. S. Wlodawski, "Photon-noise-limited operation of intensified CCD cameras," *Appl. Opt.* **36**(22), 5288–5297 (1997).
32. B. Q. Spring and R. M. Clegg, "Image analysis for denoising full-field frequency-domain fluorescence lifetime images," *J. Microsc.* **235**(2), 221–237 (2009).
33. U. Schuhle, "Intensified solid state sensor cameras: ICCD and IAPS," *ISSI Scientific Reports Series*, 419–428 (2010).
34. H. H. Barrett, R. F. Wagner, and K. J. Myers, "Correlated point processes in radiological imaging," *Proc. SPIE* **3032**, 110–124 (1997).
35. R. A. Loch, "Cesium-telluride and magnesium for high quality photocathodes: preparation and diagnostics," Master Thesis, University of Twente, Netherlands (2005).
36. R. E. Burgess, "Homophase and heterophase fluctuations in semiconducting crystals," *Discuss. Faraday Soc.* **28**, 151–158 (1959).
37. D. Kang and M. A. Kupinski, "Effect of noise on modulation amplitude and phase in frequency-domain diffusive imaging," *J. Biomed. Opt.* (in press).